

We are IntechOpen, the world's leading publisher of Open Access books Built by scientists, for scientists

6,900

Open access books available

186,000

International authors and editors

200M

Downloads

Our authors are among the

154

Countries delivered to

TOP 1%

most cited scientists

12.2%

Contributors from top 500 universities



WEB OF SCIENCE™

Selection of our books indexed in the Book Citation Index
in Web of Science™ Core Collection (BKCI)

Interested in publishing with us?
Contact book.department@intechopen.com

Numbers displayed above are based on latest data collected.
For more information visit www.intechopen.com



Insert Molding Process Employing Vapour Chamber

Jung-Chang Wang¹, Tien-Li Chang² and Ya-Wei Lee³

¹National Taiwan Ocean University,

²National Taiwan Normal University,

³National Defense University,
Taiwan, R.O.C.

1. Introduction

Insert molding process is a simplified injection molding method that eliminates secondary processing and assembly. In this process, the metal inserts are firstly formed, and placed in the mold during injection molding (the metal inserts can be designed into a grooved pattern, allowing them to be connected closely with the plastics), and then the mold is closed for injection molding. Although insert molding process can greatly improve the assembly and manufacturing procedure, the joining of two materials is the main problem yet to be solved. Because the molten plastic drives the air out of the mold cavity from the vent resulting in welding lines of a plastic part during the filling step in an injection molding process, then there will be a V-notch formed between the plastic and the mold wall if the air cannot exhaust before the melted plastic fronts meet. Thus, this chapter concerns about a V-notch found on the exterior surfaces of welding lines, which will form between the plastic and the mold wall. Not only are they appearance defects, but they also decrease the mechanical strength of the parts. Once the plastics are filled, the temperature of plastics bypassing one side of the inserts may decline more quickly than that of plastics contacting the temperature side of the mold wall, so a weld line may be formed when meeting again after bypassing the inserts. The strength at the position of weld line is generally lower than that at the region of plastics; moreover, the metal inserts are generally located at the stress region when the product is utilized. Hence, the rupture of plastics often occurs from the weld line at the rear of the metal inserts, leading to damage of products (Wang & Tsai 2011). The key approach is to rapidly and uniformly increase the temperature of inserts before the plastics enter into the mold cavity.

Some studies indicated that, during the injection molding process, the defect of weld line could be resolved by adjusting the mold temperature. The locations of the welding lines are usually decided by the part shapes and the gate locations. Welding lines can be eliminated by the following three methods. The first method is increasing the molten plastic temperature. The viscosity of the molten plastic fluid decreases with the increasing temperature, which improves the flow pattern of the plastic, and reduces the depth of the V-notch of the welding lines. However, degradation of the material strength sometimes occurred if the melting temperature is too high. The second method is increasing the number of the vents. Increasing the number of the vents (eg. ejecting pin or inserts) at the

vicinity of the welding line will dispel air from mold cavity more easily. Nevertheless, these extra vents will leave marks on the product surfaces, especially for transparent plastics. The third method is raising the mold temperature. Raising the mold temperature will increase the viscosity of the material, which in turn can reduce the depth of the V-notch. On the other hand, raised mold temperature also increases cycle time of the injection molding process, thus increases the production costs. If increased cycle time is not a problem then raise mold temperature is the simplest way for elimination of the welding lines among the three methods mentioned above.

There are several methods for raising the mold temperature. For example, replacing the water in the mold temperature controller for oil can increase the mold temperature for about 100°C. But the time required for the mold to rise to the designed temperature is too long to be practical. The mold heating is achieved by using high pressure vapour as a media in this method. When the filling stage in the injection molding process was finished, high pressure vapour was introduced for cooling. The technology does achieve a very fast heating and cooling cycle, however, its application was limited by the mold size. Wang et al. (2011a) demonstrated a vapour chamber of a two-phase flow heat transfer device consists of sealed container, wick structure and working fluid can occupy the technology easily. Its working theorem is as same as the heat pipe and generates high pressure vapour as the process of Rapid Heat Cycle Moulding (R.H.C.M.). Vapour chamber (V.C.) is verified through experiment and theory that the temperature difference between the center and edge of vapour chamber-based thermal module is within 1°C and this temperature difference for the copper Integral Heat Spreader (IHS) with the same size at the same experimental parameters are more than 6°C (Wang, 2011a). Therefore, vapour chamber represents better temperature homogeneity. In recent years, technical development related with the application of two-phase flow heat transfer assembly to thermal modules has become mature and heat pipe-based two-phase flow heat transfer module is one of the best choices (Wang & Wang, 2011). The thermal performance of a heat sink with embedded heat pipes has been developed a Windows program for rapidly calculating through Visual Basic commercial software (Wang et al., 2010b). Moreover, one set of risers of the L-shape heat pipes were functioning as the evaporating section while the other set acted as condensing section. Six L-type heat pipes are arranged vertically in such a way that the bottom acts as the evaporating section and the risers act as the condensing section (Wang, 2011c). The temperature difference is under 1°C while the percentage of the non-condensation gas is less than $8 \times 10^{-5}\%$, and the single heat pipe has the maximum heat capacity (Wang, 2011b). To establish a practical quick methodology that can effectively and efficiently determine the thermal performances of heat pipes so as to substitute the use of the conventional steady-state test. This is much more efficient than the steady-state test and would be greatly beneficial to the notebook PC industry or other heat dissipation technologies that use heat pipes.

Fig. 1 showed a heat pipe / thermal pin employed in the injection molding process over several decades. Liquid thermoplastics require the cooling inside the injected cavity. The mold must be equipped to provide the cooling surroundings. Thermal pins had become standard components to cool areas that are difficult to reach with water lines. A commercially available thermal pin with heat conductivity several magnitudes higher than core, which accomplishes better cooling effect and more uniform temperature distribution. However, thermal pin is just only one-dimensional heat conducting path. Vapour chamber

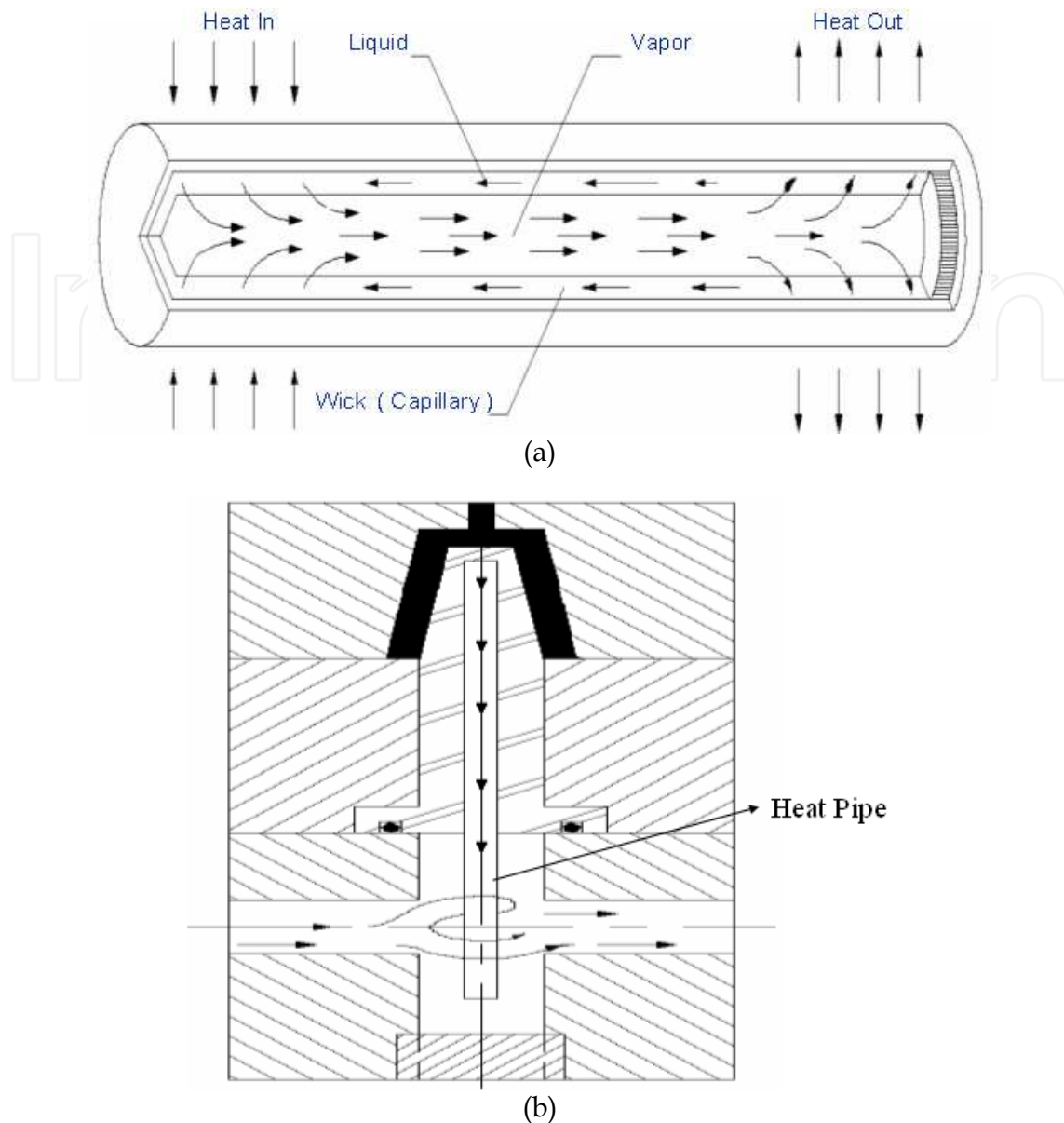


Fig. 1. Heat pipe / thermal pin for mold cooling.

may regard as many thermal pins to heat spreading area. Wang et al. (2011a) uses the local heating mechanism, along with the excellent thermal performance of vapour chamber, to analyze and enhance the strength of products formed after insert molding process. Finally, it has been found that a vapour chamber based rapid heating and cooling system for injection mold is proposed for reducing the welding lines of the transparent plastic products and enhancing their strengths through these results.

Vapour has advantages of fast, large amount and safety. The effectiveness and better thermal performance of vapour chamber has been already confirmed according up-to-date researches and mass production application in server system and VGA thermal module. Moreover, vapour chamber-based thermal module has existed in the thermal-module industry for a year or so especially in server application (Wang & Chen 2009; Wang 2010; Wang et al. 2011b). A novel formula for effective thermal conductivity of vapour chamber has been developed by use of modified dimension analysis in combination with thermal-

performance experimental method (Wang & Wang 2011). It is deduced from the novel formula that the maximum effective thermal conductivity is above $800 \text{ W/m}^\circ\text{C}$, and comparing it with the experimental value, the calculating error is no more than $\pm 5\%$. It respectively discussed these values of one, two and three-dimensional effective thermal conductivity and compared them with that of metallic heat spreader. For metallic materials as the heat spreaders, their thermal conductivities have constant values when the operating temperature is slight change. The thermal conductivities of pure copper and aluminum as heat spreaders are $401 \text{ W/m}^\circ\text{C}$ and $237 \text{ W/m}^\circ\text{C}$ at operating temperature of 27°C , respectively. When the operating temperature is 127°C , they are $393 \text{ W/m}^\circ\text{C}$ and $240 \text{ W/m}^\circ\text{C}$, respectively. The maximum heat flux of the vapour chamber is over $800,000 \text{ W/m}^2$, and its effective thermal conductivity will increase with input power increasing. Thermal performance of V.C. is closely relate to its dimensions and heat-source flux, in the case of small area vapour chamber and small heat-source flux, the thermal performance will be less than that of pure copper material.

A vapour chamber is a two-phase heat transfer components with a function of spreading and transferring uniformly heat capacity so that it is ideal for use in non-uniform heating conditions especially in LEDs (Wang 2011d). The solid-state light emitting diode (SSLED) has attracted attention on outdoor and indoor lighting lamp in recent years. LEDs will be a great benefit to the saving-energy and environmental protection in the lighting lamps region. Wang et al. (2010a) introduce a thermal-performance experiment with the illumination-analysis method to discuss the green illumination techniques requesting on LEDs as solid-state luminescence source application in relative light lamps. The temperatures of LED dies are lower the lifetime of lighting lamps to be longer until many decades. The thermal performance of the LED vapour chamber-based plate (LED-VCPCB) is many times than that of LED copper- and aluminium-based plates (Wang & Huang 2010; Wang 2011d). Wang et al. (2010a) utilizes experimental analysis with window program VCTM V1.0 to investigate the thermal performance of the vapour chamber and apply to 30 Watt high-power LEDs. Results show that the maximum effective thermal conductivity is $965 \text{ W/m}^\circ\text{C}$ at 187.5 W/cm^2 . Anyway, the chapter is divided into two parts; first part examines a vapour chamber to rapid heating and cooling system for injection molding process. Second part employs the vapour chamber system with numerical method and performance experiment to investigate the key factors affecting the performance of the Self-Contained Underwater Breathing Apparatus (SCUBA) system utilizing the insert molding process (Tsai et al. 2011).

2. Vapour chamber for rapid heating and cooling system (VC_RHCS)

Vapour Chamber (V.C.) is a two-phase heat transfer device inside vapour-liquid working, which has better thermal performance than metallic material in a large footprint heat sink. The overall operating principle of V.C. is defined as follows: at the very beginning, the interior of the vapour chamber is in the vacuum, after the wall face of the cavity absorbing the heat from its source, the working fluid in the interior will be rapidly transformed into vapour under the evaporating or boiling mechanism and fill up the whole interior of the cavity, and the resultant vapour will be condensed into liquid by the cooling action resulted from the heat convection effect between the fins and fan on the outer wall of the cavity, and reflow to the place of the heat source along the capillary structure. Thus, vapour chamber spreads large amount heat flow rapidly and is feasible to utilize in the insert molding process, which the metal insert is firstly placed into the mold, and then formed into an embedded plastic product by injection molding. Therefore, the products can be formed in a

single molding process, helping to shorten the processing time and reduce the possible human error arising from several procedures. These common defects are often found on the exterior surfaces of welding lines, which are not only appearance defects; they also decrease the mechanical strength of the parts. When the metal inserts are placed in the mold for injection molding, a weld line may be formed from the plastics after bypassing the inserts. Traditionally, the inserts are placed in the mold at room temperature, but the temperature of inserts is lower than that of the mold (the temperature of inserts cannot rise sharply within a very short period) when the filling is conducted after mold sealing.

2.1 Verification of VC_RHCS

Fig. 2 reveals the apparatus of VC_RHCS employing vapour chamber to rapid heating and cooling system for injection molding process. A local heating mechanism of vapour chamber proposed that the mold is a moveable slider, at inner side of which a heating rod is installed; a vapour chamber is mounted at the joint of the frontal edge of the slider and the mold wall. When the inserts are placed in the mold and the mold is closed, the heated slider will move forward, and contact the vapour chamber, so that the inserts are heated up rapidly and quickly with the vapour chamber. A heating and cooling system with vapour chamber was developed in this chapter. A vapour chamber was installed between the mold cavity and the heating block. The heating and cooling system used in the experiment was $50 \times 50 \times 80\text{mm}^3$. It can be incorporated with the mold at any location regardless of the mold size. The heating cycle is activated by a lever mechanism which pushes the vapour chamber to contact with the mold at the filling stage. The lever pusher is a hydraulic cylinder. Two electrical heating tubes are provided a mold steel block named P20 material and thermocouples are embedded to measure the temperature of the heat insert device. The heat source for vapour chamber is a low density cartridge heater which contact with the vapour chamber only when the lever is activated. When the filling completed, the heat source separates form the vapour chamber.

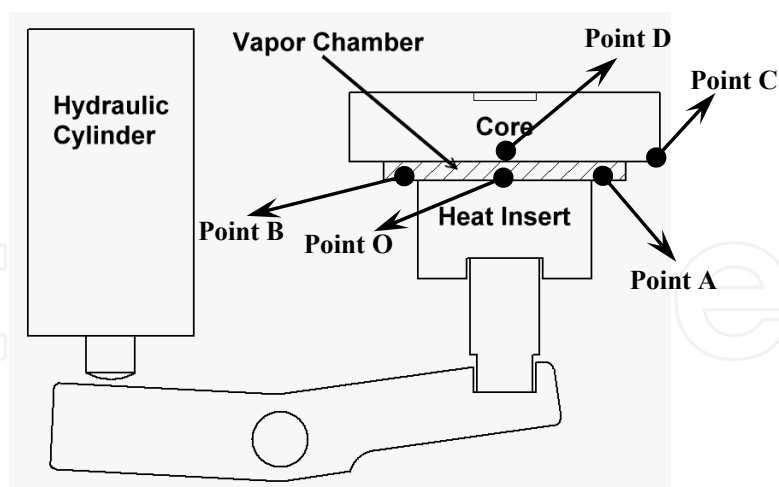


Fig. 2. Mechanics of heating and cooling cycle system with vapour chamber (VC_RHCS).

There are five thermal couples placed on the surface of cavity to measure the temperature of vapour chamber as shown in Fig. 2. Points A and B are measured the temperatures of the opposite to the position of the heat insert device on the surface of cavity. Points C and D are measured the temperature of the opposite to the position of vapour chamber on the surface of cavity. Point O is measured the central temperature of cavity and vapour chamber. And

the point C is the farthest distance away from point O. Mold temperature was raised to above the glass transition temperature of the plastic before the filling stage. Cooling of the mold was then started at the beginning of the packing stage. The entire heating and cooling device was incorporated with the mold. The capacity and size of the heating and cooling system can be changed to accommodate the mold. The plastic was ABS (Chi-Mei PA-758) in the experiment, its glass transition temperature is 109°C. The material for mold base is JIS S50C. The material for mold core is ASSAB 718. There are two injection molds estimated the products using vapour chamber and the testing material is ABS. The VC_RHCS can raise the tensile strength and reduce the defect of the welding lines of a plastic product because of rapid-uniform heating and cooling cycle with vapour chamber.

These temperature curves of zero to sixty seconds with / without vapour chamber are shown in Figs 3. In the Fig. 3(a), the temperature of point O is 73.9°C and the farthest corner away from point O is 34.7°C of point C at 60 seconds. Furthermore, temperature differences of the other points A, B, D are large values about 10°C each other at 60 seconds. In the Fig. 3(b), the temperature of point O and point C is 83.7°C and 67.8°C at 60 seconds, respectively. In addition, the temperatures of the other points A, B, D are almost 80°C at 60 seconds. The temperature curve of point O of Fig. 3(a) is faster raise than that of Fig. 3(b) at zero to thirty seconds resulting from the heater direct contact and slows down after thirty seconds. In other words, the temperature of point O of Fig. 3(a) is higher than that of Fig. 3(b) before thirty seconds. The mean temperature of these five points with vapour chamber and without vapour chamber is 78.3°C and 56.1°C, respectively. Rapid uniform temperature effect employing vapour chamber heating system is better even if the heater is direct touching point O on the surface of cavity for no vapour chamber system.

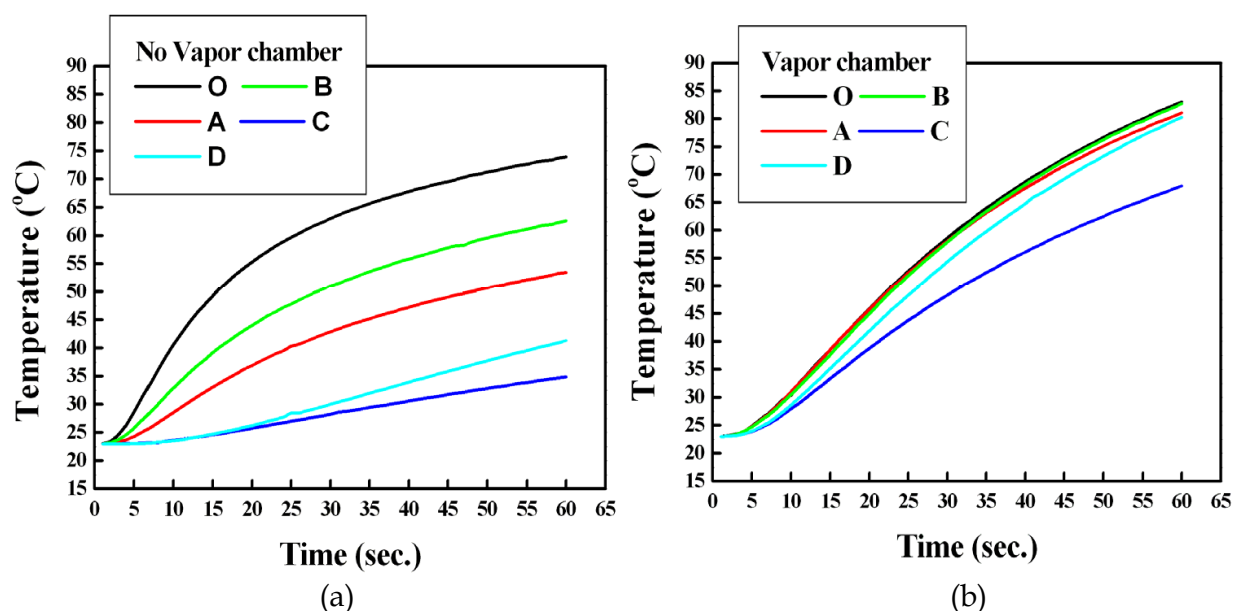


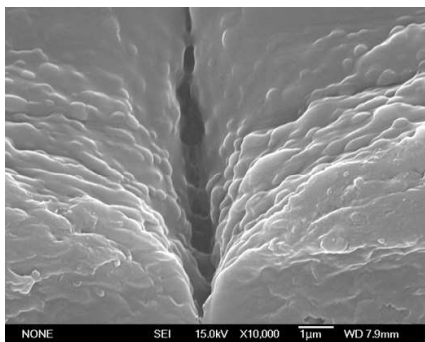
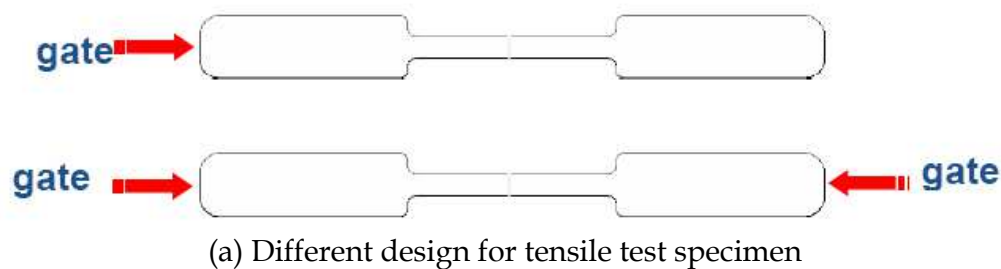
Fig. 3. Relationships of the temperatures with the heating time with/without vapour chamber.

2.2 Employing VC_RHCS in tensile testing parts

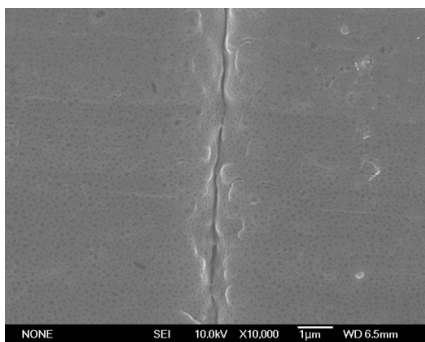
The products of the injection molding experiments were tensile testing parts. They are evaluated the effectiveness of the proposed heating and cooling system with vapour chamber and without vapour chamber. There are two different mold designs namely one

gate mold and two opposite gates mold were selected for the experiments. Fig. 3 shows the relationships of the temperature with the heating time with/without vapour chamber. If there are no the effect of vapour chamber, these five thermal couples show non-uniform on the surface of cavity. However, the dimensions of these tensile testing parts are 215.9 x 12.7 x 25.4mm³ with 3.175mm thickness.

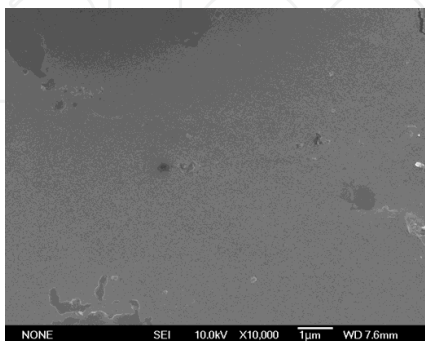
Table 1 shows the tensile strength of the products in different situation of one gate and two opposite gates with and without vapour chamber. The tensile strength supposes maximum for one gate without vapour chamber heating system because of on welding line from the Fig. 4. Fig. 4 shows the test specimen and SEM images of welding line. One gate without vapour chamber system experiments resulted tensile test pars without any welding lines. Two gates without vapour chamber heating system appears apparent welding line and its tensile strength of testing part is lower 11.1% than the part of one gate from table 1 and Fig. 4.



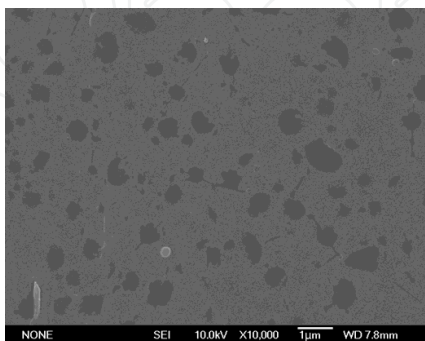
(b) Two opposite gates at the temperature of Point O is 75°C without vapour chamber system



(c) Two opposite gates at the temperature of Point O is 75°C with vapour chamber system



(d) Two opposite gates at the temperature of Point O is 110°C with vapour chamber system



(e) One gate at the temperature of Point O is 75°C without vapour chamber system

Fig. 4. SEM pictures of one gate and two opposite gates.

Condition	Max. stress (Kgf / cm ²)	Strength (%)
Two gate without vapour chamber Cavity temp. = 75°C	165	88.9
Two gate with vapour chamber Cavity temp. = 75°C	178	95.7
Two gates with vapour chamber Cavity temp. = 110°C	184	98.9
One gate without vapour chamber Cavity temp. = 75°C	186	100.0

Table 1. The results of the tensile test.

Two gates with vapour chamber heating system appears light welding line and its tensile strength of testing part is higher 6.8% than the part of two gates without vapour chamber system. If increasing the preheating temperature from 75°C to 110°C with two gates vapour chamber system, the tensile strength can again add 3.2%.

2.3 Employing VC_RHCS in eight holes test part

Another test part is the multi-holes products tested to evaluate the effectiveness of the system with vapour chamber in different situation of cavity and core temperatures. These multi-holes products have eight holes with four 10mm and 5mm diameter holes, respectively. The dimensions of eight holes products are 110 x 53 x 3.175mm³. Three temperature combinations were tested in the experiments. Case 1 is the conditions of cavity temperature 60°C and core temperature 60°C. Case 2 is the conditions of cavity temperature 60°C and core temperature 130°C. Case 3 is the conditions of cavity temperature 80°C and core temperature 130°C.

Figs. 5 show the specification of the eight holes test part and SEM images of V-notch. The means is that there are many welding lines on the surface of the transparent parts. The depth of the V-notch is deeper the welding line is more obvious for transparent. From the Figs. 5, the depths of the V-notch found on each case are 12µm, 2µm, and 0.5µm respectively. The product of the case 1 shows a V-notch 24 times deeper than the product of case 3. The effects of cavity and core temperatures are also important for welding line. Finally, utilizing VC_RHCS shows that the temperature differences of cavity employing vapour chamber are smaller than that without vapour chamber and increasing preheating temperature can add the tensile strength for two opposite gates resulting from extending enough fluid flow. And the new VC_RHCS can reduce the depth of v-notch as much as 24 times.

3. SCUBA system utilizing VC_RHCS

The underwater environment imposes many physical and mental stressors on those working in the modern SCUBA (Self-Contained Underwater Breathing Apparatus) diving equipment. A scuba system consists of a high pressure compressed air tank and a pressure regulator. The development of SCUBA diving is based on the invention of the regulator. The high pressure air carried by diver must be reduced to the pressure in the ambient environment by the regulator before the diver can breathe it. The life of the diver thus depends on the performance and stability of the regulator. The SCUBA is based on the

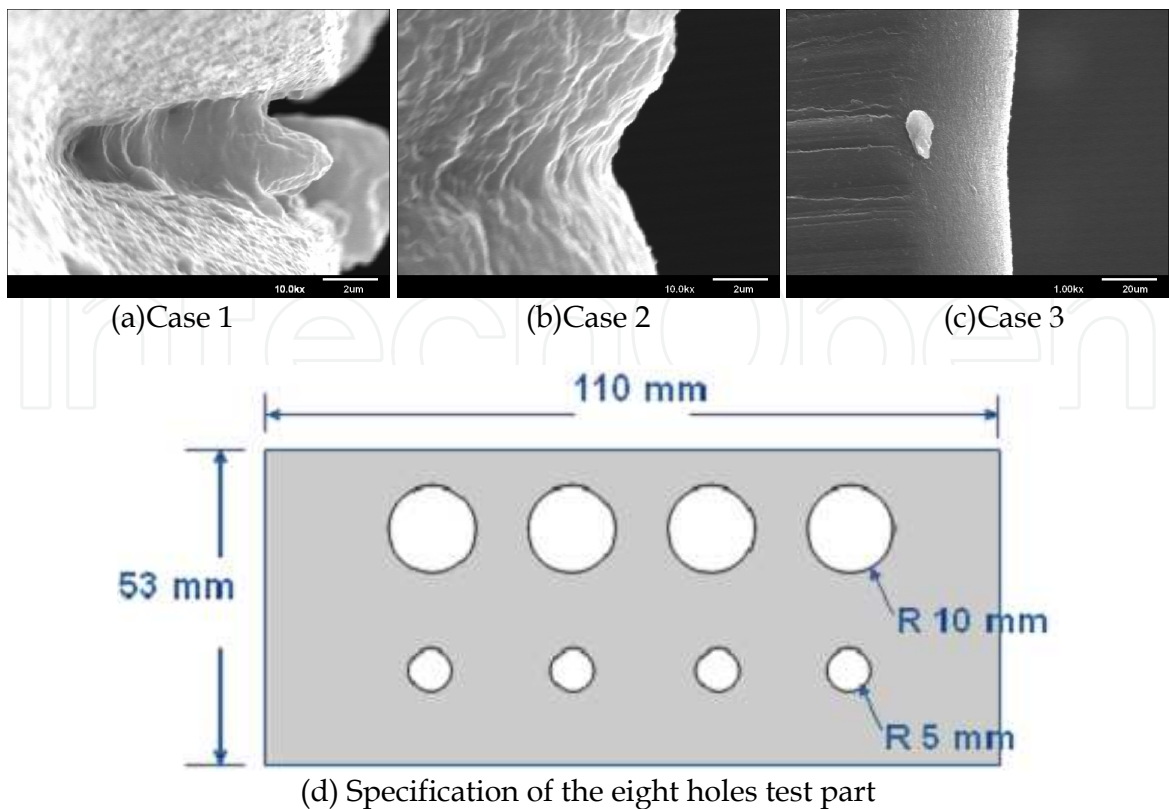


Fig. 5. SEM picture of the eight holes plate.

invention of breathing regulators. Basically, a regulator can be divided into the first and second stages. The first stage regulates air output pressure at a stable value of 14atm, reducing from the compressed air cylinder pressure of 200atm to 20atm, and then supplies that air to the second stage. The second stage is connected to the divers’ mask and supplies air at ambient pressure based on the diver’s respiration.

Underwater movement requires a higher expenditure of energy and an increased rate of respiration than the same movement on land. This is caused by the higher density of water, and the need to overcome water resistance or drag. The second stage supplies air at a pressure equivalent to water pressure, which in turn depends on the depth, in order to lessen the diver’s lung burden. A structural representation of the second stage is shown in Fig.6, while Fig. 7 gives a schematic of the second stage. The second stage of the regulator thus affects the smoothness of diver breathing, a key factor in the divers’ ability to function underwater. During this experiment, the relationship between characteristic factors and performance of breathing regulators will be explored through numerical methods, to enable designers to create more efficient breathing regulators.

Breathing resistance is directly related to the diver’s ability to receive sufficient air to safely perform in the underwater environment and must be considered a primary factor in the design of breathing apparatuses. An ideal breathing regulator allows divers to breathe without consuming additional energy when breathing under water. In other words, in the ideal regulator, respiratory work rate and respiratory impedance are zero. Many patents (Belloni 2001; Brown & Brown 2000 & 2002; Christianson 1987; Ferguson 1997; Garraffa 1997; Garraffe 1996; Hansen & Lingenfelter 1987; Houston 1981; Toth1985) involve optimum designs for breathing regulator. These patents discussed above provide researchers with a

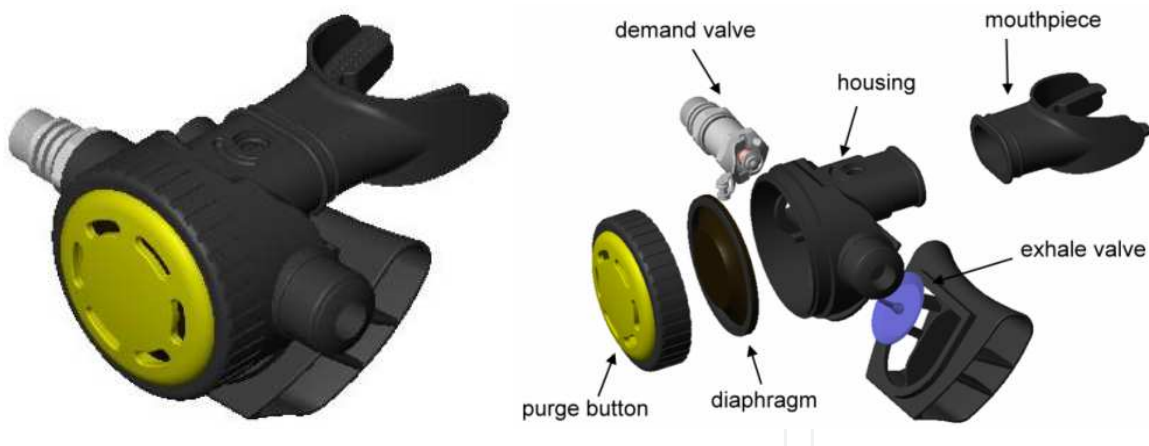


Fig. 6. The structural representation of the second stage.

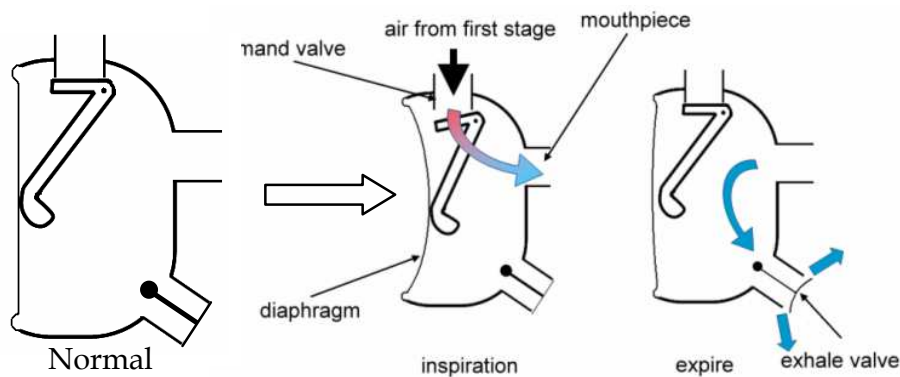


Fig. 7. The schematic diagram of the second stage.

reference for developing new breathing regulators. However, in previous studies, the parameters affecting the breathing regulator's performance have not been identified. This research identifies the design parameters affecting regulator performance through experimental and numerical methods.

The analysis is divided into two steps in this section. In the first step, the mechanical characteristics of samples are varied and the relevant performance parameters of the breathing regulators are tested using demand regulator testers made by ANSTI Co., as shown in Fig. 8. In the second step, we modify the characteristic internal shapes of the regulators and explore how these changes influence regulator functions using commercial numerical simulation software, FLOW-3D® from Flow Science Inc. Company. There are several important considerations to design of breathing regulators for diving apparatus. A regulator must meet the requirements for easy breathing and a stable air supply at normal conditions. Easy breathing is the most key index of a regulator. However, to a great extent, the above factors are shaped by the subjective feeling of the user. In order to accurately describe breathing smoothness, designers have defined two parameters, namely respiratory work rate and respiratory impedance.

The unit of respiratory work rate is Joule/Liter and its value represents the average energy consumed by breathing in and out one liter of air. Respiratory impedance can be regarded as the pressure supplied by a diver when breathing underwater. For example, in order to smoothly discharge gas through a regulator when diving, a diver must apply a pressure using the thoracic cavity and mouth to force the valves to open. To breathe in, additional

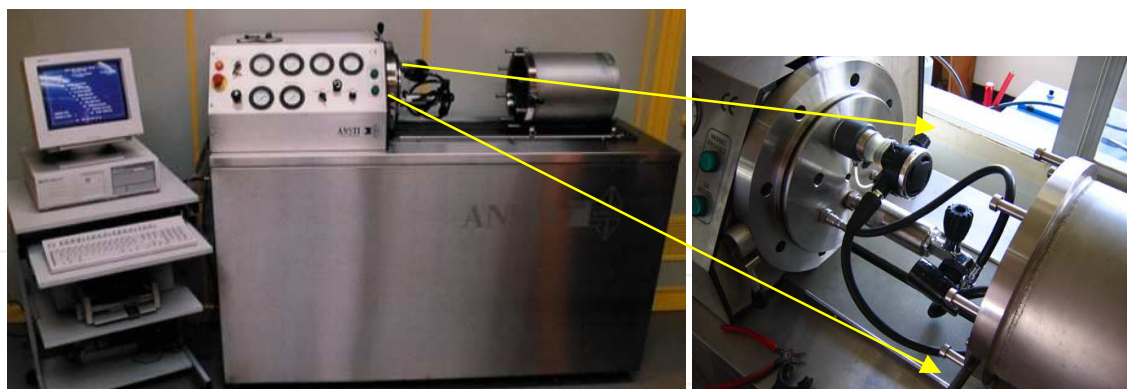


Fig. 8. The regulator testers made by ANSTI Co.

negative pressure must be produced to open the valves. These pressures are cumulatively known as respiratory impedance. Respiratory impedance values are widely used to evaluate various breathing mask products, such as filter-type dust masks and gas masks. A picture of the regulators under this study is shown in Fig. 9. A deflecting plate is located at the front end of the air inlets, whose angle can be adjusted by the user. There are two spray holes, one in the upper part and the other in the lower part, directing air flow towards the diaphragm, inside the housing. The factors under consideration in this research are the deflecting plate and the spray holes.



Fig. 9. A picture of the test regulator.

For the numerical analysis, the entire analytical model is established by utilizing file conversion skill between CAD/CFD. The overall dimension of simulation analytical model is about $30 \times 30 \times 25 \text{ cm}^3$. Schematic process of numerical simulation analysis adopted in the article can be divided into pre-processing, numerical solving and post-processing. With regard to pre-processing, first of all, a geometrical model is established for 3D CFD module. Generally, in order to reduce computation grid elements and time taken for simulation and solving, some minor characteristics without influence or with a little influence will be ignored when establishing 3D geometrical model. And input the boundary conditions and thermo-physical properties, which the ambient temperature is set to 27°C , the input pressure is set to 9 atm and initial pressure is set to be the surrounding conditions, turbulent model is the k- ϵ two-equations, the grid pattern is structural one and the entire simulation analysis type is transient time state. For the entire module, about 1,500 thousands grid

elements are used, time step is about 10^{-9} , iterations is about 50 per time-step and it will take about 14 days to simulate every scenario.

The following paragraphs will describe the functions of the three parts.

3.1 Flow channel

A flow channel functions to direct gas from the valves into the diver’s mouth. Flow channel design is thus closely related to respiratory impedance, respiratory work rate, and gas flow velocity. Fig. 10 shows three types of flow channel design for the simulation models. Model B1 represents the original design; Model B2 is a lengthened flow channel which completely covers the entire suction port, while Model B3 is short flow channel design.

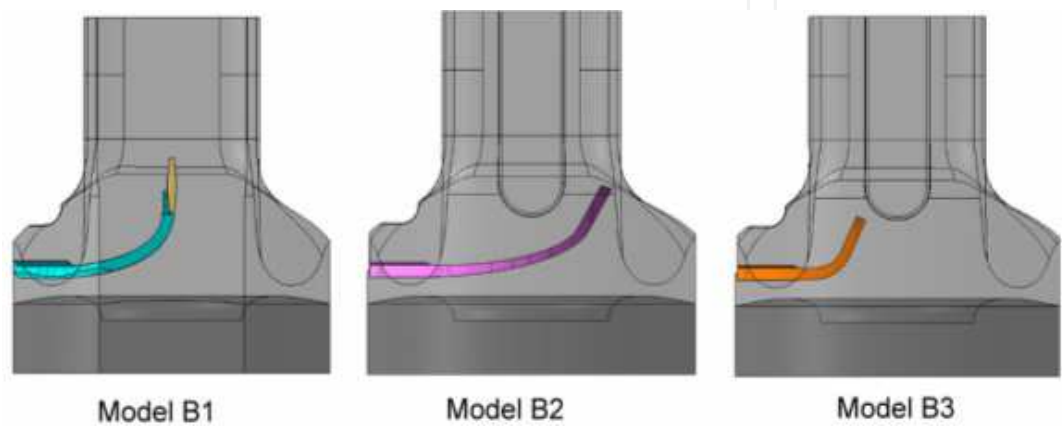


Fig. 10. The design of Model B1~B3 modified the length of the flow channel.

The analytical data is given in Table 2 and pressures obtained from the three designs are compared in Fig. 11. The offset is the difference between maximum pressure inside the housing and mouthpiece, which obtained from simulated data of FLOW-3D®. Our simulations show that when an excessively long flow channel covers the upper part of the suction port, the gas inside the housing will be blocked, unable to enter the suction end, resulting in a pressure rise inside the housing. By the same token, an excessively short flow

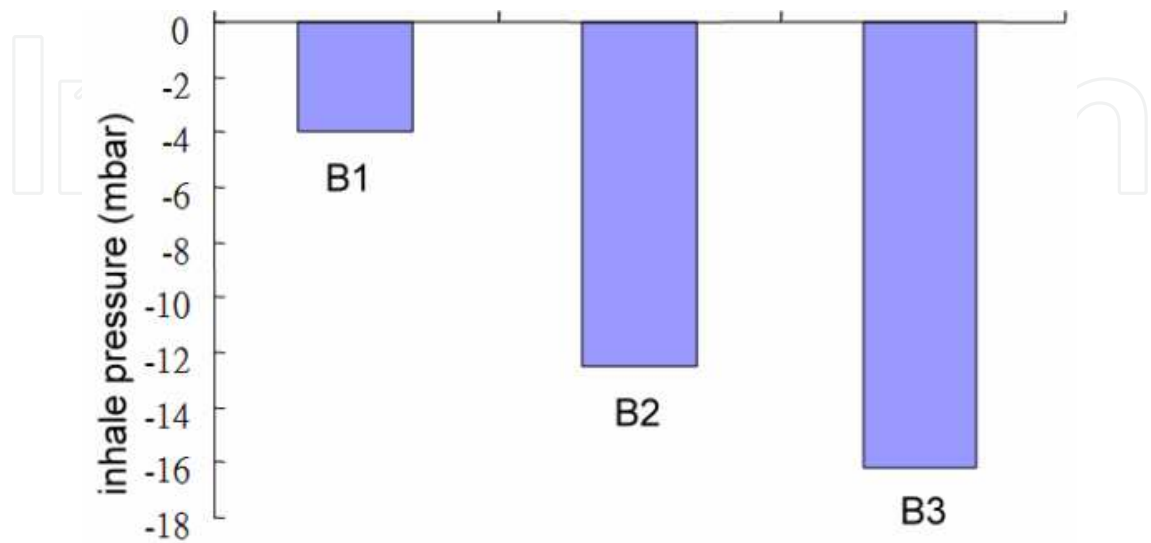


Fig. 11. Inhale pressure of different length of flow channel.

Model	pressure inside the housing (bar)	pressure in the mouthpiece (bar)	Offset (mbar)
B1	6.899	6.931	-4
B2	6.883	6.9065	-12.5
B3	7.0272	7.047	-16.2

Table 2. Comparison of different length of flow channel.

channel will cause the gas inside the flow channels to flow into the housing, creating a pressure drop at the suction end. The offset have to be close zero pressure drop. Our numerical results showed that the original design “B1” obtains the best inhale pressure.

3.2 Angle of the spray holes

After entering the second stage from the spray holes, high-speed gas strikes the diaphragm, which results in a pressure rise inside the diaphragm. A change in the angle of the spray holes will affect the spray whole’s pressure shock against the diaphragm. The authors modified the characteristics of actual samples and tested these modified samples on a tester bench. A comparison was made between experimental data and simulation values obtained by FLOW-3D® to confirm that the mode for setting boundary conditions, in which air is vented out at a constant flow rate, is consistent with actual conditions. These modifications mainly aim at the characteristics of the dimensions of period, line and depth. After confirming that the data obtained from numerical model is consistent with experimental data.

Table 3 shows the characteristics of the five groups of samples were varied across experiments (A1 to A5) in order to verify that numerical simulation data and experimental data reliable. These modifications are mainly aimed at the characteristics of deflector holes and spray holes.

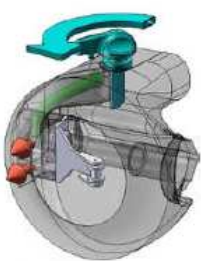
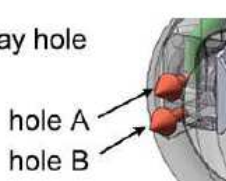
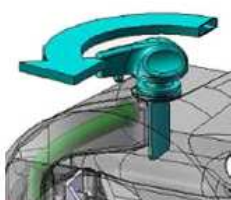
	 spray hole hole A hole B		 The angle of the flow channel
	spray open=O , close=X		
	A	B	
A1	O	O	0°
A2	X	O	0°
A3	X	X	0°
A4	X	X	22.5°
A5	X	X	45°

Table 3. The test parameters of the regulator.

As we have seen, a comparison of the experimental data and numerical simulation results is given in Table 4. And the comparison of the experimental data and the simulated data of inhale pressure are shown in Fig. 12. The results show that the simulated data are acceptably

close to the experimental data. After confirming that the data obtained from numerical model is consistent with the experimental data, the authors changed the characteristics of the second stage mechanisms and then determined how the shape characteristics affect regulator performance, using numerical simulation.

Model	pressure inside the housing (bar)	pressure in the mouth piece (bar)	Offset (mbar) (Simulated Data)	Inhale pressure measured from ANSTI test machine (mbar) (Experimental Data)
A1	7.0905	7.111	-16.4	-15.5
A2	6.899	6.931	-5	-4
A3	8.468	8.515	8.43	11
A4	6.655	6.696	5.56	5
A5	6.654	6.683	-6.89	-7

Table 4. The experimental results VS. The results of simulation.

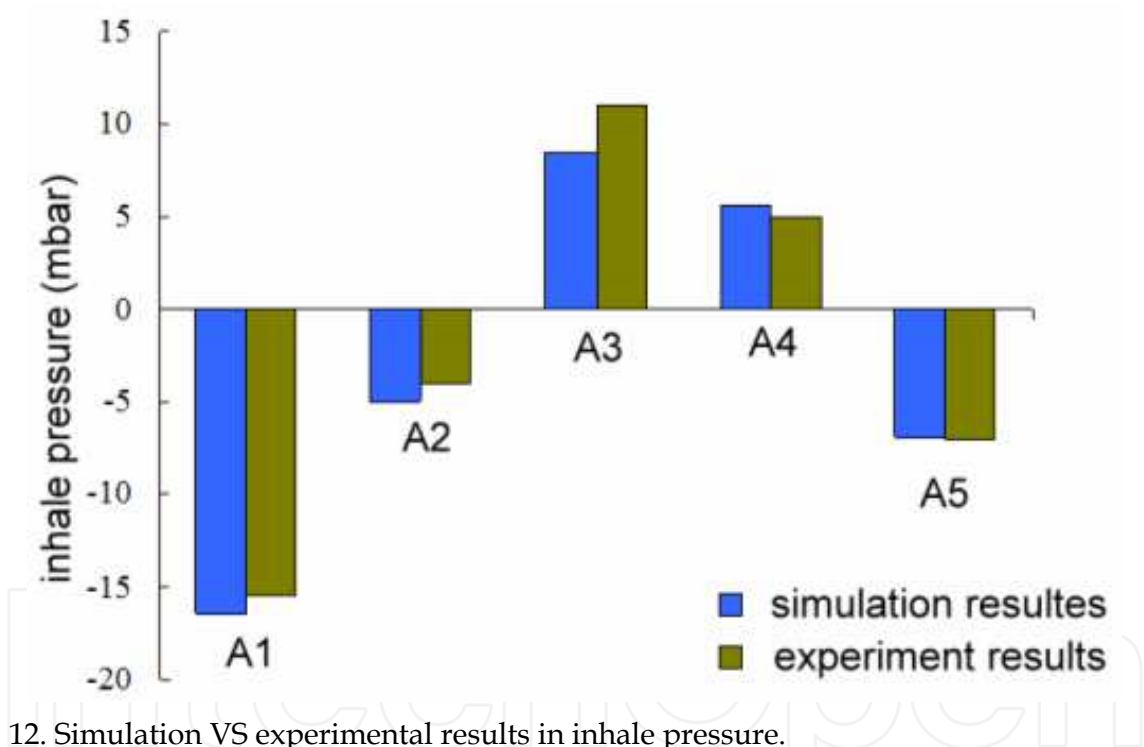


Fig. 12. Simulation VS experimental results in inhale pressure.

In our model design, Model A2 is used as a control, and the angle of its lower spray hole B is varied. Three designs are adopted, designated C1, C2 (Fig.13) and C3 (Fig.14). The key point in the C3 design is to prevent the gas from directly striking the housing and instead allow it to pass along the housing edge when gas enters the housing. The analytical data is summarized in Table 5 and a comparison is given in Fig.15. Our results are also confirmed in the stream line diagram as shown in Fig.16. At this condition, the internal pressure value can be reduced to about one-third of the pressure of the original design of Model A2. However, if the gas is not applied to the diaphragm at all after entering the housing, as in C2, the inhale pressure will become a positive value, which increases respiratory impedance. This must be avoided by the designer. Fig. 17 depicts a stream line diagram of C2.

Model	pressure inside the housing (bar)	pressure in the mouthpiece (bar)	Offset (mbar)
A2	6.4685	6.5025	-2
C1	6.6745	6.7095	-1
C2	6.623	6.665	6
C3	6.7395	6.775	-0.5

Table 5. Comparison of different angle of spray hole.

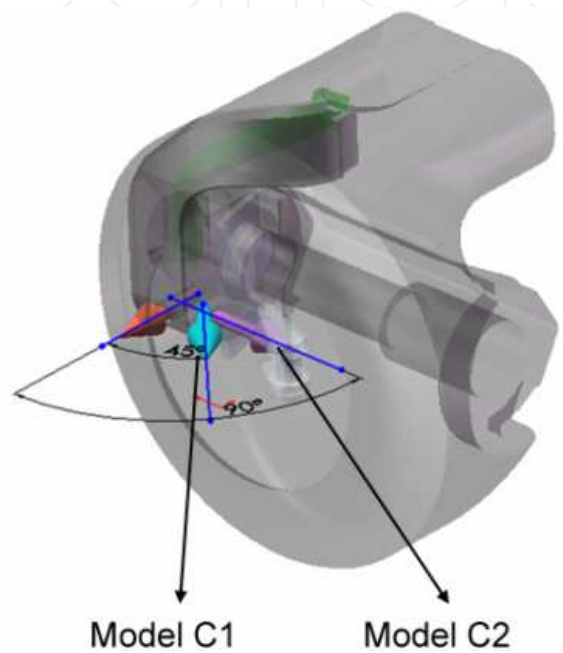


Fig. 13. Model C1 and C2 modified the direction of the spray hole.

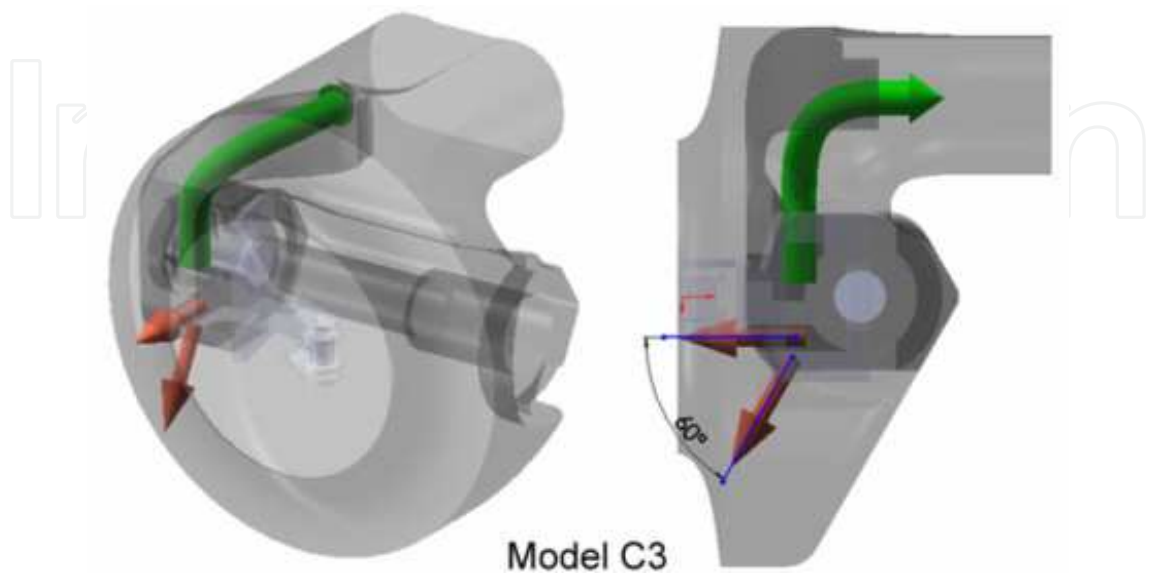


Fig. 14. Model C3 modified the direction of the spray hole.

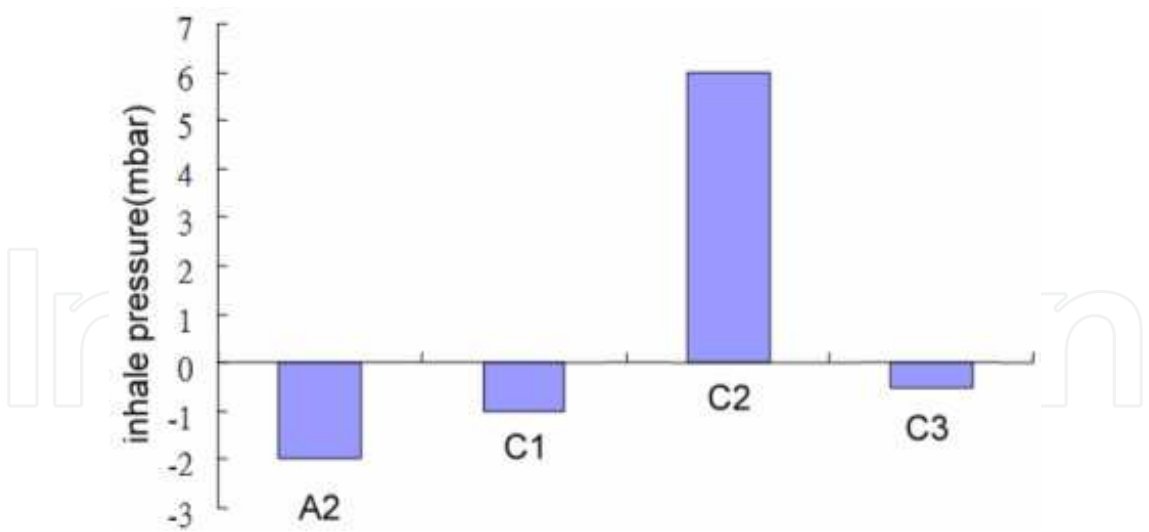


Fig. 15. The inhale pressure of different angle of spray hole.

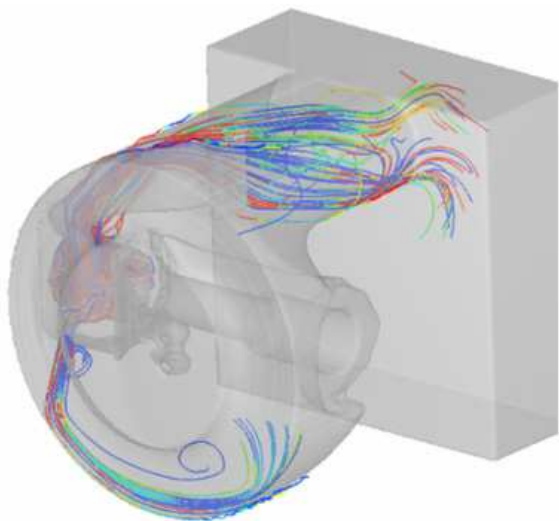


Fig. 16. The stream lines of Model C3.

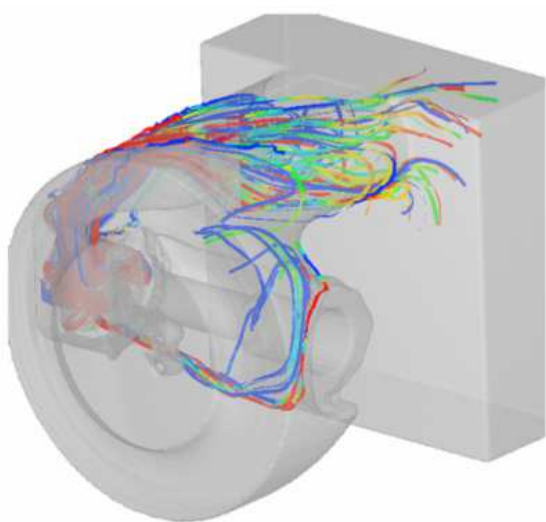


Fig. 17. The stream lines of Model C2.

3.3 Size of spray holes

The size of the spray holes will affect the flow velocity of the gas into the second stage, resulting in a change in internal pressure. The spray hole affects the pressure inside the diaphragm and housing to a great extent. When high-speed gas from the spray holes directly strikes the diaphragm, the pressure inside the diaphragm will rise. The size of the spray holes affects the gas velocity inside the housing. In this research, three groups of models, namely D1, D2 and D3, are used for testing. The position and diameters of the spray holes are shown in Fig. 18.

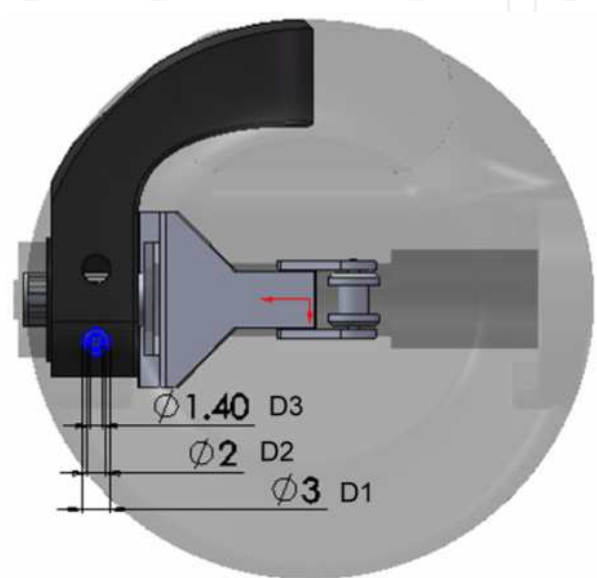


Fig. 18. Modify the size of spray hole (Model D1, D2, and D3).

The analytical data in Table 6 and Fig.19 shows that the pressure inside the housing is proportional to the hole diameter. The larger the hole diameter is, the higher the pressure inside the housing, which in turn reduces the differential pressure between the internal pressure and pressure at the suction end. However, when the hole diameter is too small (D3), the increasing differential pressure will cause the inhale pressure to change from a negative value to a positive value, thus reducing respiratory impedance. After several tests by simulation, when the spray hole diameter decreases from 2mm to 1.8mm, the inhale pressure will be reduced to one-third of the inhale pressure of the original design. In last, these experimental results can be simulated by numerical analysis software FLOW-3D®.

Model	pressure inside the housing (bar)	pressure in the mouthpiece (bar)	Offset (mbar)
D1	6.899	6.931	-4
D2	6.4685	6.5025	-2
D3	6.3835	6.3435	+4

Table 6. Comparison of different size of spray hole.

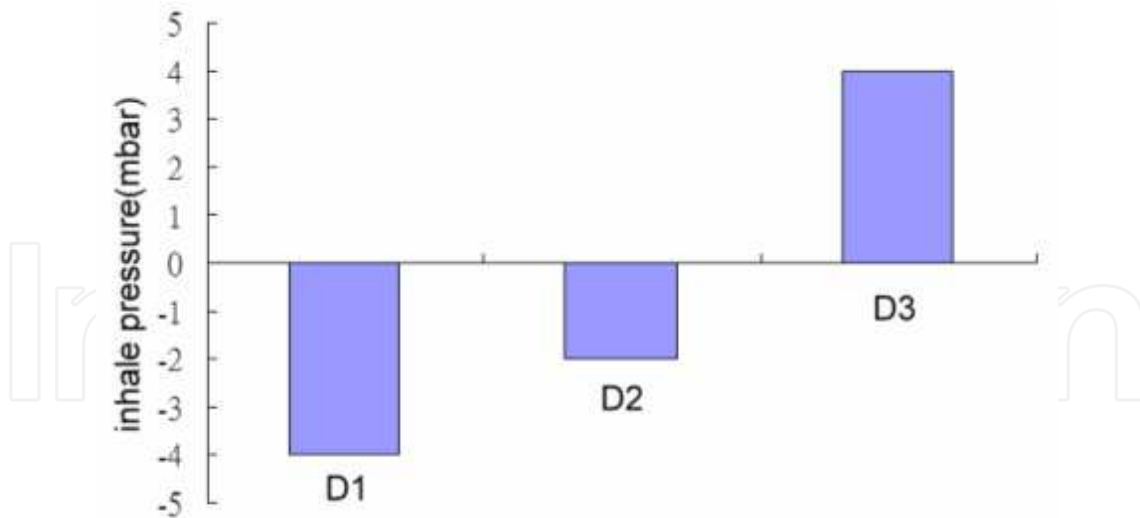


Fig. 19. The inhale pressure of different size of spray hole.

4. Conclusions

This study proved that, among existing insert molding process, the temperature of inserts has impact on the final assembly strength of product. In this chapter, the local heating mechanism of vapour chamber can control the molding temperature of inserts; and the assembly strength can be improved significantly if the temperature of inserts prior to filling can be increased over the mold temperature, thus allowing the local heating mechanism to improve the weld line in the insert molding process. A VC_RHCS for injection molding can effectively reduce the welding lines of the transparent plastic products. The heating and cooling injection molding system associated with vapour chamber can raise the tensile strength and reduce the defect of the welding lines of a plastic product because of VC_RHCS rapid-uniform heating and cooling cycle. The results show that the plastic products with two opposite gates was found increasing by 6.8% and 10% of tensile strength compared with the conventional one, and the other plastic product with eight holes plate is decreased from 12 μ m to 0.5 μ m of the depth of the welding line. And the performance of the breathing regulator can be accurately confirmed using numerical simulation software. The angle and diameter of the spray holes are key parameters affecting the performance of breathing regulators. Further, the diameter of the internal spray holes is inversely proportional to inhale pressure. These results indicate that the product formed by the VC_RHCS can effectively achieve high material strength and reduce weld line.

5. Acknowledgments

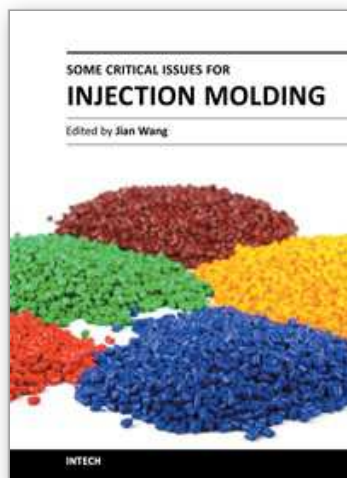
This chapter originally appeared in these References and is a minor revised version. Some of the materials presented in this chapter were first published in these References. The authors gratefully acknowledge Prof. R.-Q. Hsu and his MPDB Lab. and Dr. Y.-P. Tsai for guidance their writings to publish and permission to reprint the materials here. The work and finance were supported by National Science Council (NSC), National Taiwan Ocean University (NTOU), National Taiwan Normal University (NTNU) and National Defense University (NDU). Finally, the authors would like to thank all colleagues and students who contributed to this study in the Chapter.

6. References

- Belloni A. (2001). Regulator with bypass tube, US Patent 6,279,575.
- Brown, R.I. ; Brown, D.S. (2000). System and method to prevent the transmission of pathogenic entities between the multiple users of second stage regulators, US Patent 6,089,225.
- Brown, R.I. ; Brown, D.S. (2002). Diving regulator with valved mouthpiece, US Patent 6,354,291.
- Christianson T. (1989). Regulator second stage for scuba, US Patent 4,862,884.
- Ferguson A.R. (1997). Adjustment mechanism for a scuba second stage airflow regulator, US Patent 5,660,502.
- Garraffa D.R. (1997). Breathing regulator apparatus having automatic flow control, US Patent 5,678,541.
- Garraffe, D.R. (1996). Second stage scuba diving regulator, US Patent 5,549,107.
- Hansen H.R. ; Lingenfelter T.A. (1987). Breathing regulator mouthpiece, US Patent 4,683,881.
- Houston, C.E. (1981). Underwater breathing apparatus, US Patent 4,245,632.
- Toth D.J. (1985). Diaphragm assembly for scuba diving regulator, US Patent 4,508,118.
- Tsai, Y.-P. ; Wang, J.-C. & Hsu, R.-Q. (2011). The Effect of Vapour Chamber in an Injection Molding Process on Part Tensile Strength. *EXPERIMENTAL TECHNIQUES*, Vol. 35, No 1, January/February, 2011, pp.60-64.
- Wang, J.-C. & Chen, T.-C. (2009). Vapour chamber in high performance server. *Microsystems IEEE 2010 Print ISBN: 978-1-4244-4341-3, Packaging Assembly and Circuits Technology Conference (IMPACT), 2009 4th International*, Taipei, October, 2009, pp.364-367.
- Wang, J.-C. & Huang, C.-L. (2010). Vapour chamber in high power LEDs. *IEEE 2011 Print ISBN: 978-1-4244-9783-6, Microsystems Packaging Assembly and Circuits Technology Conference (IMPACT), 2010 5th International*, Taipei, October, 2010, pp.1-4.
- Wang, J.-C. & Tsai, Y.-P. (2011). Analysis for Diving Regulator of Manufacturing Process. *Advanced Materials Research*, Vol. 213, February, 2011, pp.68-72.
- Wang, J.-C. & Wang R.-T. (2011). A Novel Formula for Effective Thermal Conductivity of Vapour Chamber, *EXPERIMENTAL TECHNIQUES*, Vol. 35, No 5, September/October, 2011, pp.35-40.
- Wang, J.-C. (2010). Development of Vapour Chamber-based VGA Thermal Module. *International Journal of Numerical Methods for Heat & Fluid Flow*, Vol. 20, No. 4, June, 2010, pp.416-428.
- Wang, J.-C. (2011a). Applied Vapour Chambers on Non-uniform Thermo Physical Conditions. *Applied Physics*, Vol. 1, April, 2011, pp.20-26.
- Wang, J.-C. (2011b). Investigations on Non-Condensation Gas of a Heat Pipe. *Engineering*, Vol. 3, April, 2011, pp.376-383.
- Wang, J.-C. (2011c). L-type Heat Pipes Application in Electronic Cooling System. *International Journal of Thermal Sciences*, Vol. 50, No. 1, January, 2011, pp.97-105.
- Wang, J.-C. (2011d). Thermal Investigations on LEDs Vapour Chamber-Based Plates. *International Communication in Heat and Mass Transfer*, Vol.38, No. 9, November, 2011, pp. 1206-1212.
- Wang, J.-C. ; Wang, R.-T. ; Chang, C.-C. & Huang, C.-L. (2010b). Program for Rapid Computation of the Thermal Performance of a Heat Sink with Embedded Heat Pipes. *Journal of the Chinese Society of Mechanical Engineers*, Vol. 31, No. 1, January/February, 2010, pp.21-28.

- Wang, J.-C. ; Wang, R.-T.; Chang, T.-L. & Hwang, D.-S. (2010a). Development of 30 Watt High-Power LEDs Vapour Chamber-Based Plate. *International Journal of Heat and Mass Transfer*, Vol. 53, No. 19/20, September, 2010, pp.3900-4001.
- Wang, J.-C.; Li, A.-T.; Tsai,Y.-P. & Hsu, R.-Q. (2011a). Analysis for Diving Regulator Applying Local Heating Mechanism of Vapour Chamber in Insert Molding Process. *International Communication in Heat and Mass Transfer*, Vol.38, No. 2, February, 2011, pp.179-183.
- Wang, R.-T. ; Wang, J.-C. and Chang T.-L. (2011b). Experimental Analysis for Thermal Performance of a Vapour Chamber Applied to High-Performance Servers, *Journal of Marine Science and Technology-Taiwan*, Vol.19, No.4, July/August, 2011, pp.353- 360.

IntechOpen



Some Critical Issues for Injection Molding

Edited by Dr. Jian Wang

ISBN 978-953-51-0297-7

Hard cover, 270 pages

Publisher InTech

Published online 23, March, 2012

Published in print edition March, 2012

This book is composed of different chapters which are related to the subject of injection molding and written by leading international academic experts in the field. It contains introduction on polymer PVT measurements and two main application areas of polymer PVT data in injection molding, optimization for injection molding process, Powder Injection Molding which comprises Ceramic Injection Molding and Metal Injection Molding, and some special techniques or applications in injection molding. It provides some clear presentation of injection molding process and equipment to direct people in plastics manufacturing to solve problems and avoid costly errors. With useful, fundamental information for knowing and optimizing the injection molding operation, the readers could gain some working knowledge of the injection molding.

How to reference

In order to correctly reference this scholarly work, feel free to copy and paste the following:

Jung-Chang Wang, Tien-Li Chang and Ya-Wei Lee (2012). Insert Molding Process Employing Vapour Chamber, Some Critical Issues for Injection Molding, Dr. Jian Wang (Ed.), ISBN: 978-953-51-0297-7, InTech, Available from: <http://www.intechopen.com/books/some-critical-issues-for-injection-molding/insert-molding-process-employing-vapor-chamber>

INTECH
open science | open minds

InTech Europe

University Campus STeP Ri
Slavka Krautzeka 83/A
51000 Rijeka, Croatia
Phone: +385 (51) 770 447
Fax: +385 (51) 686 166
www.intechopen.com

InTech China

Unit 405, Office Block, Hotel Equatorial Shanghai
No.65, Yan An Road (West), Shanghai, 200040, China
中国上海市延安西路65号上海国际贵都大饭店办公楼405单元
Phone: +86-21-62489820
Fax: +86-21-62489821

© 2012 The Author(s). Licensee IntechOpen. This is an open access article distributed under the terms of the [Creative Commons Attribution 3.0 License](https://creativecommons.org/licenses/by/3.0/), which permits unrestricted use, distribution, and reproduction in any medium, provided the original work is properly cited.

IntechOpen

IntechOpen